Reprinted from Journal of the Optical Society of America B, Vol. 5, page 1520, July 1988

Spectra in the 60–345-Å wavelength region of the elements Fe, Ni, Zn, Ge, Se, and Mo injected into the Princeton Large Torus tokamak

A. Wouters, J. L. Schwob,* and S. Suckewer

Princeton Plasma Physics Laboratory, Princeton University, Princeton, New Jersey 085

J. F. Seely and U. Feldman

E. O. Hulburt Center for Space Research, Naval Research Laboratory, Washington, D.C. 20375-5000

J. H. Davé

Applied Research Corporation, 8201 Corporate Drive, Landover, Maryland 20785

Received January 4, 1988; accepted March 8, 1988

High-resolution spectra of the elements Fe, Ni, Zn, Ge, Se, and Mo injected into the Princeton Large Torus tokamak were recorded by the 2-m Schwob–Fraenkel soft-x-ray multichannel spectrometer. Spectra were recorded every 50 msec during the times before and after injection. The spectral lines of the injected element were very strong in the spectrum recorded immediately after injection, and the transitions in the injected element were easily distinguished from the transitions in the intrinsic elements (C, O, Ti, Cr, Fe, and Ni). An accurate wavelength scale was established using well-known reference transitions in the intrinsic elements. The spectra recorded just before injection were subtracted from the spectra recorded after injection, and the resulting spectrum was composed almost entirely of transitions from the injected element. A large number of $\Delta n = 0$ transitions between the ground and the first excited configurations in the Li I through K I isoelectronic sequences of the injected elements were identified in the wavelength region 60 to 345 Å.

INTRODUCTION

The Princeton Large Torus (PLT) tokamak is a useful tool for the study of the spectra of highly charged ions. Electron temperatures up to 2.5 keV occur in the center of the ohmically heated discharge and persist for as long as 1 sec. Since this time period is typically long compared with the ionization and recombination times of the highly charged ions from the wall material, the spectra of these ions are essentially steady during most of the plateau regime of the discharge. The spectra of transiently injected elements are easily detected against the steady background spectra of the intrinsic elements.

Time-resolved spectra of the intrinsic elements (C, O, Ti, Cr, Fe, and Ni) and of injected elements have been recorded with the 2-m Schwob–Fraenkel soft-x-ray multichannel spectrometer (SOXMOS). Spectra were recorded every 50 msec in the 60–345-Å wavelength region. Corrections were made for nonlinearities in the multichannel detector and the fiber-optic transmission line, and an accurate wavelength scale was established, using well-known reference lines. The spectra from the intrinsic elements were presented in Ref. 1. In the present paper we present the spectra of the injected elements Fe, Ni, Zn, Ge, Se, and Mo.

EXPERIMENTAL CONFIGURATION

The spectra of the injected elements were recorded by the SOXMOS spectrometer[2–4] fitted with a 600-line/mm grating and a blaze angle of 3° 31′. The spectra were detected by a flat MgF_2-coated microchannel plate (MCP) that was coupled to a 1024-pixel photodiode array by a fiber-optic transmission line. For each discharge, data in a wavelength interval approximately 50 Å wide could be recorded, and the wavelength region from 60 to 345 Å was covered by moving the MCP. Spectral scans were recorded every 50 msec throughout the discharge, and typically more than 10 usable scans with strong spectral features were obtained on each discharge.

The elements were injected during the plateau regime of ohmically heated discharges using the laser blowoff technique. Before the time of injection, the recorded spectra were composed of transitions in highly charged ions of the elements from the wall material (C, O, Ti, Cr, Fe, and Ni). We shall refer to the spectrum of the intrinsic elements as the background spectrum.

Shown in Fig. 1 are the spectra in the wavelength region 155 to 215 Å recorded just before and after Mo injection. The spectrum shown in Fig. 1(a) was recorded just before injection and is composed of transitions from the intrinsic elements. In the spectrum recorded 50 msec later, Fig. 1(b), transitions from highly charged Mo ions appear superimposed upon the background spectrum. The Mo transitions are diminished in the next spectrum, recorded 50 msec later [Fig. 1(c)].

The spectra shown in Fig. 1 are typical of the spectra of the injected elements. In general, the intensity of the back-

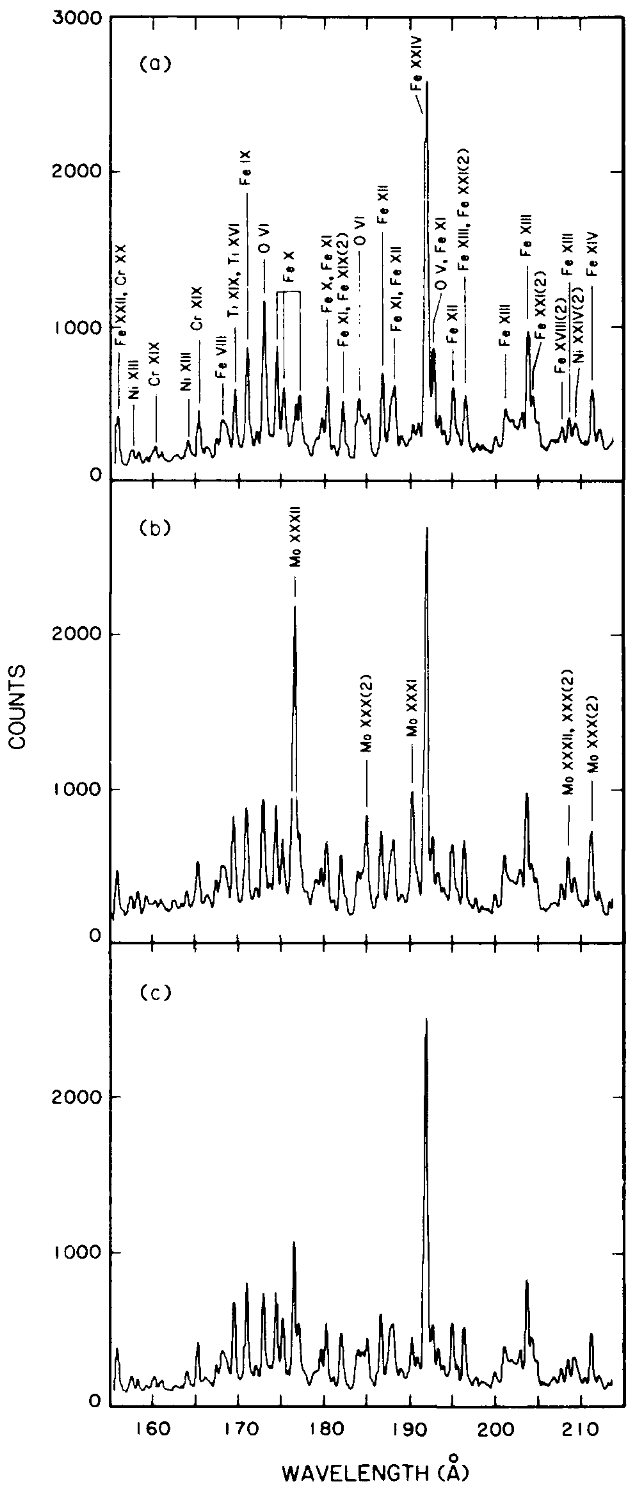

Fig. 1. Spectra recorded at intervals of 50 msec during a PLT discharge. Spectrum (a) was recorded just before injection, and spectra (b) and (c) were recorded after injection of Mo.

ground continuum and line intensities increases slightly during injection, probably because of the increased electron density, but the background spectrum is otherwise not significantly perturbed. The transitions from the injected element appear strong in the spectral scans recorded immediately after injection and diminish during the following several scans. Since the relative intensities of the background spectral features do not vary significantly during injection, it is possible to difference the scans recorded before and after injection and thereby suppress the background spectrum. This is illustrated in Figs. 2–5 for the case of Mo injection. For example, the spectrum shown in Fig. 4 was obtained by subtracting the spectrum of Fig. 1(a) from the spectrum of Fig. 1(b). The difference spectrum is composed almost entirely of transitions from the injected element. In some cases, the relative intensities of some background transitions may vary slightly during injection, but this variation is always small. This is illustrated in Fig. 4, where the O VI transition at 173.0 Å decreased during injection and appears below the continuum level in the difference spectrum.

MEASURED WAVELENGTHS

The wavelength scale was established using transitions from the intrinsic elements recorded before injection. The basic

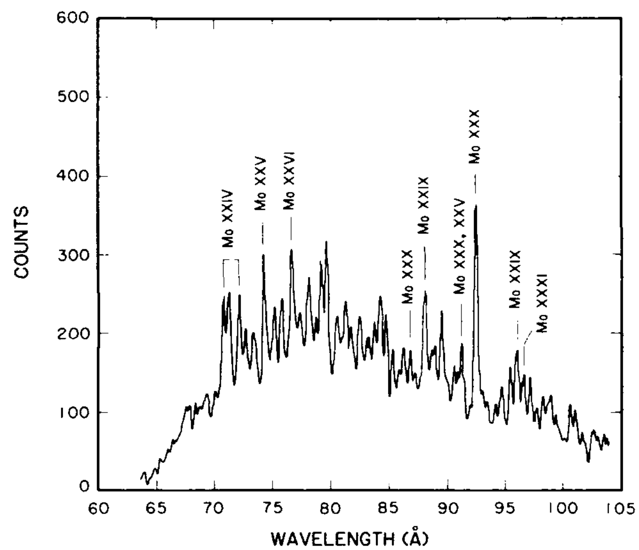

Fig. 2. Mo spectrum in the wavelength region 60–105 Å.

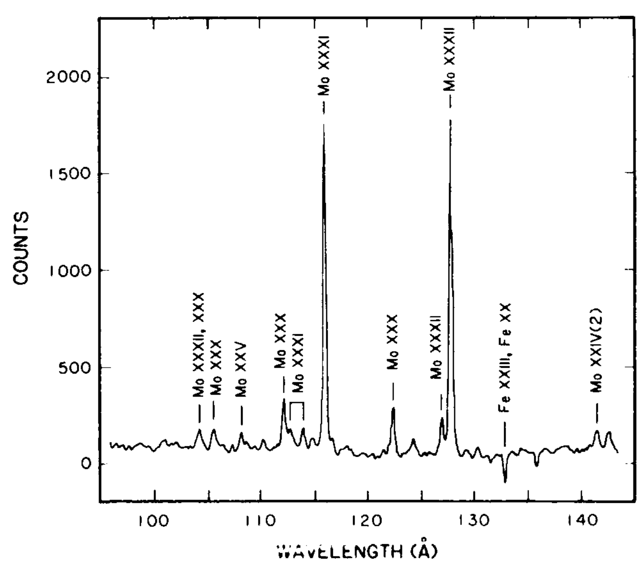

Fig. 3. Mo spectrum in the wavelength region 95–145 Å.

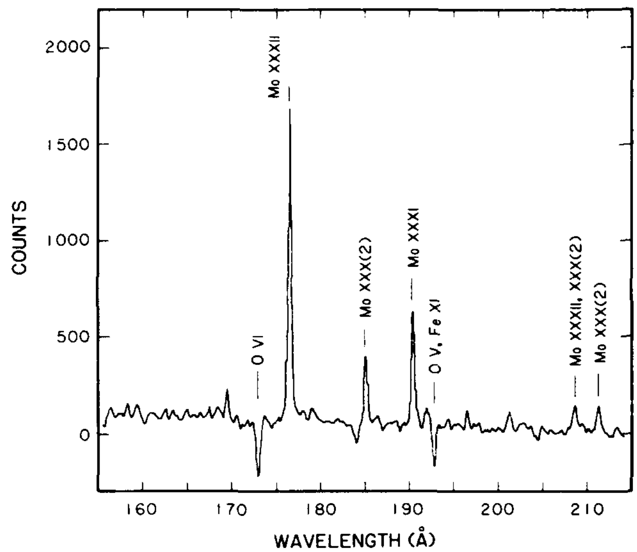

Fig. 4. Mo spectrum in the wavelength region 155–215 Å.

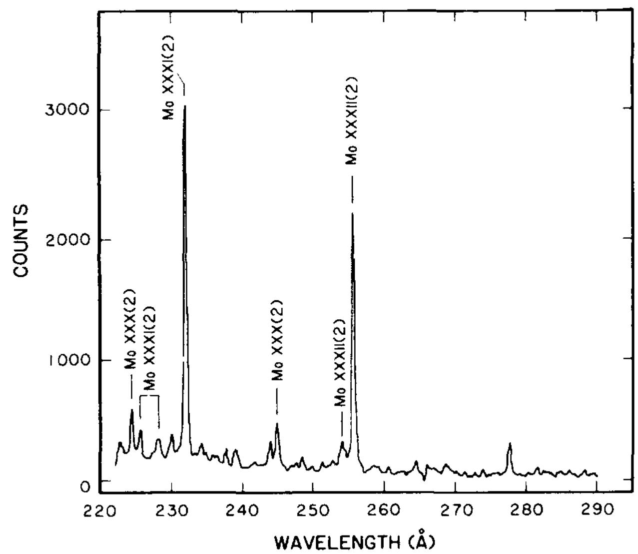

Fig. 5. Mo spectrum in the wavelength region 220–295 Å.

technique for establishing the wavelength scale was described in Ref. 1. In the present work, several improvements in this technique have been made.

The wavelength of a spectral feature is given by the grating equation

$$\lambda = d(\cos\alpha - \cos\beta), \tag{1}$$

where d^{-1} is the number of lines per unit length of grating, α is the angle of incidence, and β is the angle of diffraction. As derived in Ref. 1, the effective angular position β of a pixel p on the MCP, measured from the angular position β_0 of the tangential pixel p_0, is

$$\beta = \beta_0 + \cot^{-1}[(2RN/M)/(p - p_0) + \cot\beta_0] \qquad \text{for } p \neq p_0, \tag{2}$$

where R is the radius of the Rowland circle, M is the magnification of the fiber-optic transmission line, and N is the number of pixels per unit length on the detector. The angle β_0 of the tangential pixel changes when the MCP is moved along the Rowland circle to cover different wavelength regions. The tangential pixel is ideally fixed at the midpoint of the MCP at pixel number 512, and the quantity RN/M is also fixed. By using the known wavelengths and expected pixel positions of the reference transitions in the background spectrum, it is possible to correct for nonlinearities in the fiber optic and the pixel array. The correction curve is ideally characteristic of the MCP and detector and is independent of the MCP position on the Rowland circle. This was the approach used in Ref. 1. In the present work it was found that the correction curves derived from spectra recorded at different MCP positions varied slightly. After the uncertainties in the measured positions of the reference transitions were taken into account, the variation in the correction curve was greater than expected and was attributed to slight changes in the geometry of the spectrometer. For example, the tangential pixel, which is nominally the midpoint of the detector at pixel number 512, may change owing to slight imperfections in the MCP carriage and guide. The effective radius of the Rowland circle R may also change slightly for the same reason. In the present work the best values for the quantities RN/M, p_0, and β_0 in Eq. (2) were determined for each plasma discharge by a least-squares fit to the reference transitions.

The wavelength scale was determined as follows. The pixel positions of the spectral features in the background spectra recorded before injection were determined. A computer program determined the centroid of each spectral feature, and the wavelengths of the spectral features were calculated, using initial values for RN/M, p_0, and β_0. These initial wavelengths were typically accurate to ±0.1 Å. The calculated wavelengths were matched to a list of reference wavelengths. The list of reference transitions was essentially the same as the list in Ref. 1 with a few improvements. Typically 20–30 reference lines could be initially identified, and the quantities RN/M, p_0, and β_0 were varied to minimize the differences between the calculated and reference wavelengths. On each iteration, additional spectral features were identified, and the process continued until all the features in the background spectrum were identified. The total number of background features identified depended on the density of spectral features in a given wavelength region and was typically 40–60. When the final values of RN/M, p_0, and β_0 were used, the differences between the calculated and reference wavelengths of strong and unblended features were less than ±0.02 Å. The wavelength discrepancies for a few reference features were consistently larger than ±0.05 Å, and these reference wavelengths were removed from the list. It was found that the pixel positions of reference features recorded near the large-pixel-number end of the MCP consistently deviated from the expected pixel positions by as many as 8 pixels. This was also found in the earlier work (see Fig. 2 of Ref. 1) and is attributable to a relatively large nonlinearity in this MCP or fiber optic near the large-pixel-number end. In order to correct for this discrepancy, an *ab initio* pixel correction 0.04 $(p - 800)$ was added to the initial pixel position p for all pixels above 800. The final absolute wavelength scale is believed to be accurate to ±0.01 Å across the entire MCP.

Table 1. Classification of Spectral Lines, Currently Measured Wavelengths, and Previous Wavelengths

Transition	Wavelengths (in Angstroms)											
	Pres.	Prev.	Pres.	Prev.	Pres.	Prev.	Pres.	Prev.	Pres.	Prev.	Pres.	Prev.
Li I												
	Fe XXIV		Ni XXVI		Zn XXVIII		Ge XXX		Se XXXII		Mo XL	
$2s$–$2p$												
$^2S_{1/2}$–$^2P_{3/2}$	192.04	192.01[a]	165.39	165.38[a]	142.40	142.44[b]	122.76[b]	122.66[a]	–	105.64[a]		
$^2S_{1/2}$–$^2P_{1/2}$	255.16	255.08[a]	234.10	234.09[a]	–	215.99[a]	–	200.18[a]	–	186.25[a]		
Be I												
	Fe XXIII		Ni XXV		Zn XXVII		Ge XXIX		Se XXXI		Mo XXXIX	
$2s^2$–$2s2p$												
$^1S_0$–$^1P_1$	132.90	132.88[a]	117.98[b]	117.94[a]	104.57[b]	104.67[a]	92.78	92.81[a]	–	82.18[a]		
$^1S_0$–$^3P_1$	263.71	263.74[a]	238.89	238.86[a]	217.66	217.66[a]	–	199.46[a]	–	183.75[a]		
B I												
	Fe XXII		Ni XXIV		Zn XXVI		Ge XXVIII		Se XXX		Mo XXXVIII	
$2s^22p$–$2s2p^2$												
$^2P_{1/2}$–$^2P_{3/2}$	100.75	100.77[c]	–	87.46[c]	–	75.82[c]	–	65.64[c]	–	56.74[c]		
$^2P_{1/2}$–$^2P_{1/2}$	102.22[b]	102.22[c]	–	88.61[c]	–	76.8[c]	–	66.4[c]	–	57.3[c]		
$^2P_{3/2}$–$^2P_{3/2}$	114.39	114.41[c]	102.10[b]	102.10[c]	–	91.17[c]	–	81.37[c]	–	72.55[c]		
$^2P_{3/2}$–$^2P_{1/2}$	116.25	116.27[c]	103.68[d]	103.68[c]	–	92.6[c]	–	82.6[c]	–	73.5[c]		
$^2P_{1/2}$–$^2S_{1/2}$	117.19	117.18[c]	104.61	104.63[c]	93.62	93.5[c]	–	83.5[c]	–	74.6[c]		
$^2P_{1/2}$–$^2D_{3/2}$	135.80	135.76[c]	118.55	118.47[c]	103.70	103.60[c]	90.64	90.73[c]	–	79.56[c]		
$^2P_{3/2}$–$^2D_{5/2}$	156.00	155.94[c]	138.78	138.73[c]	–	123.20[c]	–	109.04[c]	–	96.12[c]		
C I												
	Fe XXI		Ni XXIII		Zn XXV		Ge XXVII		Se XXIX		Mo XXXVII	
$2s^22p^2$–$2s2p^3$												
$^3P_0$–$^3S_1$		91.27[e]	79.96	79.97[e]	–	70.02[e]	61.16	61.21[e]	–	53.41[e]		
$^3P_1$–$^3S_1$	97.91	97.86[e]	87.64	87.67[e]	78.71	78.71[f]	70.67	70.74[e]	–	63.55[e]		
$^1D_2$–$^1P_1$	98.32[b]	98.36[e]	87.98[d]	87.99[e]	–	78.89[e]	–	70.79[e]	–	63.52[e]		
$^3P_2$–$^1D_2$	99.06	99.03[e]	–	87.53[e]	77.13	77.11[f]	–	67.66[e]	–	59.05[e]		
$^3P_2$–$^3S_1$	102.22[b]	102.21[e]	91.87	91.87[e]	82.62	82.64[f]	74.39	74.30[f]	–	66.72[e]		
$^3P_0$–$^3P_1$	–	108.11[e]	92.71	92.72[e]	79.39	79.46[e]	67.97	68.07[e]	–	58.32[e]		
$^1D_2$–$^1D_2$	113.34[b]	113.29[e]	102.10[b]	102.07[e]	–	92.15[e]	83.21	83.14[e]	–	74.80[e]		
$^3P_1$–$^3P_0$	118.65[b]	118.69[e]	–	104.70[e]	–	92.52[e]	–	81.84[e]	–	72.42[e]		
$^3P_2$–$^3P_2$	121.19	121.19[e]	106.04[b]	106.05[e]	92.79	92.85[f]	–	81.37[f]	–	71.56[e]		
$^3P_2$–$^3P_1$	123.85	123.82[e]	–	109.09[e]	–	96.11[e]	–	84.66[e]	–	74.57[e]		
$^3P_0$–$^3D_1$	128.64	128.73[e]	111.84	111.83[e]	97.43	97.45[f]	85.12	85.08[e]	–	74.49[e]		
$^3P_1$–$^3D_2$	142.13	142.14[e]	126.62	126.59[e]	113.01	112.98[e]	100.72	100.82[e]	–	89.77[e]		
$^3P_2$–$^3D_3$	145.68	145.70[e]	128.36	128.32[e]	–	112.93[e]	–	99.28[e]	–	87.19[e]		
$^1D_2$–$^3D_3$	178.92	178.85[e]	162.18	162.19[e]	–	148.32[e]	–	136.60[e]	–	126.54[e]		
N I												
	Fe XX		Ni XXII		Zn XXIV		Ge XXVI		Se XXVIII		Mo XXXVI	
$2s^22p^3$–$2s2p^4$												
$^2D_{5/2}$–$^2P_{1/2}$	83.23	83.23[g]	–	72.52[g]	63.28	63.33[g]	–	55.38[g]	–	48.46[g]		
$^2D_{3/2}$–$^2P_{3/2}$	90.54	90.59[g]	–	80.56[g]	71.87	71.92[f]	–	64.34[g]	–	57.68[g]		
$^2D_{5/2}$–$^2P_{3/2}$	–	93.78[g]	84.09	84.07[g]	75.52	75.50[f]	–	67.84[f]	–	60.90[g]		
$^2D_{3/2}$–$^2S_{1/2}$	94.59	94.64[g]	–	84.25[g]	75.33[b]	75.29[f]	–	67.43[f]	–	60.40[g]		
$^4S_{3/2}$–$^2D_{3/2}$	95.95	95.92[g]	–	85.03[g]	75.33[b]	75.31[g]	–	66.51[g]	–	58.50[g]		
$^2P_{3/2}$–$^2P_{1/2}$	98.32[b]	98.35[g]	88.02	88.01[g]	–	78.96[f]	–	70.99[f]	–	63.83[g]		
$^2D_{3/2}$–$^2D_{3/2}$	110.59	110.63[g]	98.17	98.18[g]	87.67	87.69[f]	–	78.70[f]	–	70.87[g]		
$^2D_{5/2}$–$^2D_{5/2}$	113.34[b]	113.35[g]	100.60	100.61[g]	89.52	89.47[f]	–	79.64[f]	–	70.84[g]		
$^4S_{3/2}$–$^4P_{1/2}$	118.65[b]	118.68[g]	103.33	103.31[g]	90.06	90.05[f]	–	78.56[g]	–	68.70[g]		
$^4S_{3/2}$–$^4P_{3/2}$	121.87	121.84[g]	106.04[b]	106.05[g]	92.23	92.18[f]	–	80.08[f]	–	69.51[g]		
$^4S_{3/2}$–$^4P_{5/2}$	132.90[b]	132.84[g]	117.98[b]	117.92[g]	104.57[b]	104.54[f]	–	92.47[g]	–	81.60[g]		
O I												
	Fe XIX		Ni XXI		Zn XXIII		Ge XXV		Se XXVII		Mo XXXV	
$2s^22p^4$–$2s2p^5$												
$^1D_2$–$^1P_1$	91.01	91.01[a]	81.71	81.70[a]	–	73.59[a]	–	66.38[a]	–	59.88[a]	–	39.16[a]
$^3P_2$–$^3P_1$	101.56	101.56[a]	88.85	88.82[a]	77.93	77.95[a]	–	68.61[a]	–	60.58[a]	–	37.73[a]
$^1S_0$–$^1P_1$	106.12	106.11[a]		97.15[a]	–	89.79[a]	–	83.63[a]	–	78.33[a]	–	62.29[a]
$^3P_1$–$^3P_0$		106.32[a]	93.91	93.93[a]	83.15	83.22[a]	–	73.88[a]	–	65.67[a]	–	41.17[a]
$^3P_2$–$^3P_2$	108.34	108.36[a]	95.87[b]	95.86[a]	85.02	85.02[a]	–	75.51[a]	–	67.12[a]	–	41.99[a]
$^3P_0$–$^3P_1$	109.93	109.95[a]	96.82	96.80[a]	–	85.29[a]	–	75.21[a]	–	66.41[a]	–	11.04[a]
$^3P_1$–$^3P_1$	111.76	111.70[a]	100.27	100.24[a]	90.55	90.58[a]	–	82.38[a]	–	75.39[a]	–	55.93[a]
$^3P_1$–$^3P_2$	120.03	119.99[a]	109.26	109.31[a]	100.27	100.28[a]	92.44	92.53[a]	–	85.81[a]	–	65.83[a]

(continued overleaf)

Table 1. Continued

Transition	Wavelengths (in Angstroms)											
	Pres.	Prev.	Pres.	Prev.	Pres.	Prev.	Pres.	Prev.	Pres.	Prev.	Pres.	Prev.
F I												
	Fe XVIII		Ni XX		Zn XXII		Ge XXIV		Se XXVI		Mo XXXIV	
$2s^22p^5$–$2s2p^6$												
$^2P_{3/2}$–$^2S_{1/2}$	93.89	93.93[a]	83.20	83.18[a]	73.91	73.94[a]	–	65.90[a]	58.85[d]	58.84[a]	–	37.66[a]
$^2P_{1/2}$–$^2S_{1/2}$	103.91	103.94[a]	94.51	94.50[a]	86.55	86.54[a]	–	79.75[a]	–	73.87[a]	–	56.54[a]
Na I												
	Fe XVI		Ni XVIII		Zn XX		Ge XXII		Se XXIV		Mo XXXII	
$3s$–$3p$												
$^2S_{1/2}$–$^2P_{3/2}$	335.41	335.40[h]	292.00	291.99[i]	256.40	256.37[i]	226.53	226.50[i]	201.01	201.02[i]	127.86	127.87[i]
$^2S_{1/2}$–$^2P_{1/2}$	–	360.76[h]	320.55	320.57[i]	288.14	288.18[i]	261.47	261.50[i]	239.13	239.12[i]	176.64	176.65[i]
$3p$–$3d$												
$^2P_{1/2}$–$^2D_{3/2}$	251.09	251.07[h]	220.43	220.42[i]	195.43	195.38[i]	174.50[b]	174.39[i]	156.43	156.45[i]	104.29[b]	104.29[i]
$^2P_{3/2}$–$^2D_{5/2}$	262.98	262.98[h]	233.78	233.76[i]	210.18	210.16[i]	190.65	190.61[i]	174.10	174.10[i]	126.99	126.98[i]
$^2P_{3/2}$–$^2D_{3/2}$	–	265.00[i]	–	236.33[i]	213.20	213.33[i]	194.47	194.43[i]	178.61	178.61[i]	134.64	134.62[i]
$3d$–$4f$												
$^2D_{5/2}$–$^2F_{7/2}$	66.36	66.36[i]	52.73[d]	52.72[i]	42.91[d]	42.92[i]	35.61[d]	35.64[i]	–	30.08[i]	–	17.15[i]
$3s$–$4p$												
$^2S_{1/2}$–$^2P_{3/2}$	50.36	50.35[j]	41.03[d]	41.02[k]	33.97[d]	34.04[l]	–	28.71[l]				
$3p$–$4d$												
$^2P_{3/2}$–$^2D_{5/2}$	54.76	54.73[j]	–	44.35[j]	36.72[d]	36.71[l]	30.87[d]	30.89[l]				
$3p$–$4s$												
$^2P_{3/2}$–$^2S_{1/2}$	63.70	63.72[j]	–	51.04[k]	–	41.82[l]	–	34.92[l]				
$4d$–$5f$												
$^2D_{5/2}$–$^2F_{7/2}$	144.21	144.25[m]	–	114.74[m]								
$4f$–$5g$												
$^2F_{7/2}$–$^2G_{9/2}$	156.90	156.88[m]	124.02	124.04[m]								
Mg I												
	Fe XV		Ni XVII		Zn XIX		Ge XXI		Se XXIII		Mo XXXI	
$3s^2$–$3s3p$												
$^1S_0$–$^1P_1$	284.15	284.16[h]	249.21	249.18[h]	220.59	220.58[n]	196.55	196.57[o]	176.05	175.92[o]	116.02	115.99[p]
$^1S_0$–$^3P_1$	–	417.26[h]	–	366.82[q]	326.44	–	293.20[b]	293.4[r]	265.84	265.7[r]	190.43	190.5[r]
$3s3p$–$3s3d$												
$^3P_0$–$^3D_1$	224.79	224.75[s]	197.39	197.39[t]	–	175.02[o]	–	–	–	–	–	–
$^3P_1$–$^3D_2$	227.22	227.21[h]	199.84	199.87[t]	–	177.66[n]	–	159.14[o]	–	–	96.58	96.56[u]
$^3P_2$–$^3D_3$	233.79	233.86[h]	207.43	207.50[t]	186.31	186.35[n]	168.92	168.90[o]	154.14	154.04[o]	112.77	112.65[p]
$^1P_1$–$^1D_2$	243.79	243.79[h]	215.90[b]	215.89[t]	193.33	193.39[n]	174.50[b]	174.78[o]	158.93	158.86[o]	113.99	113.90[p]
Al I												
	Fe XIV		Ni XVI		Zn XVIII		Ge XX		Se XXII		Mo XXX	
$3s^23p$–$3s^23d$												
$^2P_{1/2}$–$^2D_{3/2}$	211.33	211.32[h]	185.20	185.22[h]	164.06[b]	164.15[n]	146.51[b]	146.52[v]	131.61	131.66[v]	86.86	86.86[v]
$^2P_{3/2}$–$^2D_{5/2}$	219.13	219.12[h]	194.01	194.04[w]	173.94	173.99[n]	157.49	157.55[v]	143.61	143.65[v]	104.29[b]	104.33[v]
$^2P_{3/2}$–$^2D_{3/2}$	220.06	220.08[h]	195.26	195.27[w]	175.57	175.52[n]	159.31	159.25[v]	145.76	145.80[v]	105.65	105.59[v]
$3s^23p$–$3s3p^2$												
$^2P_{1/2}$–$^2P_{3/2}$	–	252.20[h]	218.44	218.39[w]	190.67	190.71[n]	167.57	167.49[v]	147.67	147.63[v]	92.53	92.55[v]
$^2P_{1/2}$–$^2P_{1/2}$	257.38	257.39[h]	223.08	223.09[w]	194.68	194.80[n]	170.75	170.81[v]	150.32[b]	150.34[v]	91.27[b]	91.3[v]
$^2P_{3/2}$–$^2P_{3/2}$	264.78	264.79[h]	232.50	232.49[w]	206.24	206.24[n]	184.36	184.34[v]	165.75	165.64[v]	–	114.08[v]
$^2P_{3/2}$–$^2P_{1/2}$	270.48	270.52[h]	237.85	237.87[w]	210.88	211.03[n]	188.47[b]	188.37[v]	168.98[b]	169.06[v]	112.23[b]	112.16[v]
$^2P_{1/2}$–$^2S_{1/2}$	–	274.20[h]	239.50	239.53[w]	211.67	211.60[n]	188.47[b]	188.42[v]	168.98[b]	168.87[v]	112.23[b]	112.17[v]
$^2P_{1/2}$–$^2D_{3/2}$	334.22	334.17[h]	288.18	288.17[x]	–	249.34[n]	220.96	220.88[v]	194.54	194.44[v]	122.37	122.40[v]
$^2P_{3/2}$–$^2D_{5/2}$	–	353.83[h]	309.11	309.18[x]	–	272.09[n]	242.76	242.8[v]	216.91	216.86[v]	140.78	140.77[v]
Si I												
	Fe XIII		Ni XV		Zn XVII		Ge XIX		Se XXI		Mo XXIX	
$3s^23p^2$–$3s3p^3$												
$^3P_0$–$^3S_1$	240.71	240.71[h]	209.25	209.18[w]	183.47	183.51[n]						
$^3P_1$–$^3S_1$	–	246.21[h]	215.90[b]	215.94[w]	191.54	191.57[n]						
$^3P_2$–$^3S_1$	251.98	251.95[h]	221.93	221.93[w]	197.45	197.58[n]						
$^1D_2$–$^1P_1$	256.42	256.42[A]	–	224.04[u]	–	–						
$3s^23p^2$–$3s^23p3d$												
$^1D_2$–$^1F_3$	196.56	196.53[h]	173.67	173.73[w]	155.70	155.75[n]	141.20	–	129.06[b]	–	96.04	–
$^3P_1$–$^3D_2$	200.09	200.02[h]	–	174.99[u]	–	155.04[n]						
$^3P_1$–$^3D_1$	201.17	201.12[h]	176.10	176.10[w]	–	162.21[n]						
$^3P_0$–$^3P_1$	202.02	202.04[h]	176.64	176.69[h]	–	150.85[n]						
$^3P_2$–$^3D_2$	203.82[b]	203.79[h]	178.81	178.87[u]	–	158.98[n]						
$^3P_2$–$^3D_3$	203.82[b]	203.83[h]	179.23	179.27[h]	159.43	159.47[n]	142.93	143.04[v]	129.06[b]	129.5[y]	88.12	88.3[z]
$^3P_2$–$^3D_1$	204.97	204.94[h]	–	180.06[u]	–	–						

Table 1. Continued

Transition	Wavelengths (in Angstroms) Pres.	Prev.	Pres.	Prev.	Pres.	Prev.	Pres.	Prev.	Pres.	Prev.	Pres.	Prev.
$^1S_0$–$^1P_1$	208.67	208.68[h]	–	184.06	–	165.03[n]						
$^3P_2$–$^3P_2$	213.76	213.77[h]	189.20	189.21[u]	–	169.69[n]						
$^1D_2$–$^1D_2$	221.81	221.82[l]	195.51	195.52[u]	–	–						
P I												
	Fe XII		Ni XIV		Zn XVI		Ge XVIII		Se XX		Mo XXVIII	
$3s^23p^3$–$3s^23p^2(^3P)3d$												
$^2D_{3/2}$–$^2F_{5/2}$	186.84[b]	186.86[A]										
$^2D_{5/2}$–$^2F_{7/2}$	186.84[b]	186.88[h]	164.12	164.13[h]	146.17	146.23[n]	131.16	131.3[y]	119.05	119.7[y]		
$^2P_{3/2}$–$^2D_{5/2}$	191.08	191.05[h]	168.33	168.37[u]								
$^4S_{3/2}$–$^4P_{3/2}$	193.48	193.51[h]	–	169.68[h]								
$^4S_{3/2}$–$^4P_{5/2}$	195.14	195.12[h]	171.38	171.36[h]	152.38	152.40[n]	136.70	136.7[y]	123.38	123.3[y]		
$3s^23p^3$–$3s^23p^2(^1D)3d$												
$^2P_{1/2}$–$^2P_{3/2}$	198.60	198.56[h]		173.74[u]								
S I												
	Fe XI		Ni XIII		Zn XV		Ge XVII		Se XIX		Mo XXVII	
$3p^4$–$3p^3(^4S)3d$												
$^3P_2$–$^3D_2$	–	178.06[h]	155.09	155.12[q]	137.13	137.06[n]						
$^3P_2$–$^3D_3$	180.35[b]	180.40[h]	157.65[b]	157.73[s]	–	139.85[n]	125.04	125.0[y]	112.38	112.5[y]		
$^3P_0$–$^3D_1$	181.10	181.13[h]	–	158.77[u]	–	–						
$^3P_1$–$^3D_2$	182.16	182.17[h]	159.97[b]	159.97[u]	–	142.74[n]						
$3p^4$–$3p^3(^2D)3d$												
$^1D_2$–$^1F_3$	179.80	179.76[h]	157.65[b]	157.55[u]	–	140.43[n]	126.52	126.4[y]	113.94	114.0[y]		
$^1D_2$–$^1D_2$		184.79[h]	161.57	161.56[u]	143.74	143.68[n]						
$^3P_1$–$^3P_1$	189.12	189.12[h]	–	–								
$^3P_1$–$^3P_2$	192.80	192.81[h]	–	169.59[u]								
$3p^4$–$3p^3(^2P)3d$												
$^3P_2$–$^3P_2$	201.63	201.58[s]			151.72	151.77[n]						
Cl I												
	Fe X		Ni XII		Zn XIV		Ge XVI		Se XVII		Mo XXVI	
$3p^5$–$3p^4(^3P)3d$												
$^2P_{3/2}$–$^2D_{5/2}$	174.53	174.53[h]	152.12	152.15[s]	134.71	134.80[n]	120.81	120.9[y]	109.19	109.1[y]	76.73	76.6[z]
$^2P_{1/2}$–$^2D_{3/2}$	175.28	175.28[h]	152.88	152.95[u]	135.60	135.59[n]	–	121.8[y]	–	109.9[y]	–	80.0[z]
$^2P_{3/2}$–$^2P_{3/2}$	177.21	177.24[h]	154.15	154.18[s]	136.30	136.31[n]	121.79	-	109.97[b]	-	-	75.2[z]
$3p^5$–$3p^4(^1D)3d$												
$^2P_{3/2}$–$^2S_{1/2}$	184.50	184.54[h]	160.53	160.56[u]	138.28[b]	138.18[n]					–	78.4[z]
$^2P_{1/2}$–$^2S_{1/2}$	190.03	190.04[h]		166.88[u]		145.03[n]						
$^2P_{3/2}$–$^2D_{3/2}$	230.10	230.13[s]										
$^2P_{3/2}$–$^2P_{1/2}$					174.75	174.76[s]					–	72.7[z]
$3p^5$–$3p^4(^1S)3d$												
$^2P_{1/2}$–$^2D_{3/2}$					153.71	153.69[n]						
$^2P_{3/2}$–$^2D_{3/2}$											–	79.3[z]
Ar I												
	Fe IX		Ni XI		Zn XIII		Ge XV		Se XVII		Mo XXV	
$3p^6$–$3p^53d$												
$^1S_0$–$^1P_1$	171.07	171.07[h]	148.35	148.37[s]	130.99	131.06[n]	117.23	117.25[w]	105.85	105.9[y]	74.20[C]	74.1[z]
$^1S_0$–$^3D_1$		217.10[h]	186.99	186.98[B]	164.06[b]		145.77		131.06		91.27[b]	
$^1S_0$–$^3P_1$	244.84	244.91[h]	211.44	211.44[B]	186.13		166.41		150.32[b]		108.25	
K I												
	Fe VIII		Ni X		Zn XII		Ge XIV		Se XVI		Mo XXIV	
$3p^63d$–$3p^53d^2(^3F)$												
$^2D_{3/2}$–$^2D_{3/2}$	167.53	167.49[h]	144.26	144.21[s]	126.74	126.74[n]	112.94	112.96[w]	101.69	102.2[y]	70.80	70.7[z]
$^2D_{5/2}$–$^2D_{5/2}$	168.20	168.17[h]	144.98	144.99[s]	127.63	127.62[n]	113.81	113.93[w]	102.69	102.6[y]	72.12	72.1[z]
$^2D_{5/2}$–$^2F_{7/2}$	185.17	185.22[h]	158.34	158.37[D]	138.28[b]	138.42[n]	122.76[b]	122.82[w]	109.97[b]	109.9[y]		75.0[z]
$^2D_{3/2}$–$^2F_{5/2}$		186.61[h]	159.97[b]	159.98[D]	140.10	140.12[n]						78.9[z]
$3p^63d$–$3p^53d^2(^3P)$												
$^2D_{5/2}$–$^2P_{3/2}$	168.53	168.55[h]	145.80	145.78[D]		128.01[n]					71.24	71.2[z]

[a] B. Edlén, Ref. 27.
[b] Blend.
[c] B. Edlén, Ref. 28.
[d] Measured in second order.
[e] B. Edlén, Ref. 30.
[f] Behring *et al.*, Ref. 20.
[g] B. Edlén, Ref. 29.
[h] Behring *et al.*, Ref. 11.
[i] Reader *et al.*, Ref. 25.
[j] Edlén, Ref. 31.
[k] Feldman *et al.*, Ref. 26.
[l] Kononov *et al.*, Ref. 14.
[m] Lawson and Peacock, Ref. 21.
[n] Sugar and Kaufman, Ref. 23.
[o] Fawcett and Hayes, Ref. 10.
[p] Reader, Ref. 18.
[q] Peacock *et al.*, Ref. 19.
[r] Finkenthal *et al.*, Ref. 16.
[s] Behring *et al.*, Ref. 6.
[t] Fawcett *et al.*, Ref. 8.
[u] Burkhalter *et al.*, Ref. 12.
[v] Hinnov *et al.*, Ref. 22.
[w] Fawcett and Hayes, Ref. 7.
[x] Fawcett and Hatter, Ref. 15.
[y] Stratton *et al.*, Ref. 17.
[z] Finkenthal *et al.*, Ref. 24.
[A] Bromage *et al.*, Ref. 13.
[B] Svensson *et al.*, Ref. 9.
[C] Measured in third order.
[D] Goldsmith and Fraenkel, Ref. 5.

The wavelengths of the spectral features in the injected spectra were calculated using the final values of RN/M, p_0, and β_0 determined from the background spectra on each discharge. The background spectrum was subtracted as discussed above. A computer program measured the centroids of the spectral features, and the wavelengths were calculated using Eqs. (1) and (2). The line widths of the spectral features were 0.1 to 0.3 Å, and the maximum uncertainty in the determined wavelengths was ±0.02 Å for intense and unblended features.

LINE IDENTIFICATIONS

The identification of the spectral features in the injected spectra was based on previous observations[5-26] or on the recommended wavelengths of Edlén.[27-31] The identifications and wavelengths are presented in Table 1. Transitions in the isoelectronic sequences Li I through K I have been identified. With the exception of several Na I transitions, all these transitions are of the type $\Delta n = 0$ and terminate on levels within the ground configurations of the ions.

Nearly all the transitions in Fe, Ni, and Zn were identified. A number of transitions in Ge, Se, and Mo remain to be identified. These unidentified transitions generally fall at short wavelengths (see Fig. 2 for Mo) and are probably transitions in the Si I through K I isoelectronic sequences. The unambiguous identification of these transitions depends on the comparison of observed and calculated wavelengths along the isoelectronic sequence, and this will be the subject of future papers. This future work will also include more recently recorded data for selected elements up to Yb ($Z = 70$). Such a comparison of observed wavelengths and wavelengths calculated using the Grant[32] program has been done for three Ar-like transitions and for the Mg-like $3s^2\,{}^1S_0$–$3s3p\,{}^3P_1$ transition,[33] and these identifications are included in Table 1. The Ar I ${}^1S_0$–${}^3D_1$ and ${}^1S_0$–${}^3P_1$ transitions for Zn, Ge, Se, and Mo represent new identifications.

CONCLUSIONS

Numerical techniques were developed to analyze the spectra from the SOXMOS spectrometer. An accurate wavelength scale was established, using reference transitions in the spectrum of the intrinsic elements recorded before injection. The wavelengths of transitions from the injected elements Fe, Ni, Zn, Ge, Se, and Mo were measured, and a large number of $\Delta n = 0$ transitions were identified. The accurately measured wavelengths will permit the identification of additional transitions in the Si I through K I isoelectronic sequences of the elements Ge, Se, and Mo. The numerical techniques and isoelectronic analyses will also be applied to the spectra of selected elements up to $Z = 70$ that were recently recorded.

ACKNOWLEDGMENT

This research was supported by the U.S. Department of Energy.

* Present address, Racah Institute, Hebrew University of Jerusalem, 91904 Jerusalem, Israel.

Note added in proof: The wavelengths of four transitions in the Mg I and Ar I sequences of elements from Cu to Mo were recently reported by J. Sugar, V. Kaufman, and W. Rowan, J. Opt. Soc. Am. B 4, 1927 (1987). These wavelengths typically agree with our wavelengths to within 0.03 Å.

REFERENCES

1. J. Davé, U. Feldman, J. F. Seely, A. Wouters, S. Suckewer, E. Hinnov, and J. L. Schwob, "Time-resolved spectra in the 80–340 Å wavelength region from PLT tokamak plasmas," J. Opt. Soc. Am. B **4**, 635 (1987).
2. A. S. Filler, J. L. Schwob, and B. S. Fraenkel, "Extreme grazing incidence spectrometer with interferometric adjustment for high resolution," in *Proceedings of the 5th International Conference on VUV Radiation Physics, Castex*, M. Pouey and N. Pouey, eds. (Centre National de la Recherche Scientifique, Paris, 1977), Vol. 3, p. 86.
3. J. L. Schwob, A. Wouters, S. Suckewer, and M. Finkenthal, "High-resolution duo-multichannel soft x-ray spectrometer for tokamak plasma diagnostics," Rev. Sci. Instrum. **58**, 1601 (1987).
4. J. L. Schwob, A. Wouters, S. Suckewer, F. P. Boody, and M. Finkenthal, "Time-resolved spectra in the 5–300 Å region emitted from the PLT and TFTR tokamak plasmas," in *Proceedings of the 8th International Colloquium on EUV and X-Ray Spectroscopy of Astrophysical and Laboratory Plasmas* (International Astronomical Union, Washington, D.C., 1984), Colloquium 86.
5. S. Goldsmith and B. S. Fraenkel, "Classification of new multiplets in the extreme-ultraviolet spectra of nickel, copper, and zinc," Astrophys. J. **161**, 317 (1970).
6. W. E. Behring, L. Cohen, and U. Feldman, "The solar spectrum: wavelengths and identifications from 60 to 385 angstroms," Astrophys. J. **175**, 493 (1972).
7. B. C. Fawcett and R. W. Hayes, "The classification of Ni XI to XVII and Co X to XVII emission lines from $3s^23p^n$–$3s3p^{n+1}$ and $3p^n$–$3p^{n-1}3d$ transitions and the identification of nickel solar lines," J. Phys. B **5**, 366 (1972).
8. B. C. Fawcett, R. D. Cowan, and R. W. Hayes, "New classifications of highly ionized Ni, Co, Cr, V, and isoelectronic spectra," J. Phys. B **5**, 2143 (1972).
9. L. A. Svensson, J. O. Ekberg, and B. Edlén, "The identification of Fe IX and Ni XI in the solar corona," Solar Phys. **34**, 173 (1974).
10. B. C. Fawcett and R. W. Hayes, "Spectra in the period between copper and bromine produced with the aid of a 4-GW laser," J. Opt. Soc. Am. **65**, 623 (1975).
11. W. E. Behring, L. Cohen, U. Feldman, and G. A. Doschek, "The solar spectrum: wavelengths and identifications from 160 to 770 angstroms," Astrophys. J. **203**, 521 (1976).
12. P. G. Burkhalter, J. Reader, and R. D. Cowan, "Spectra of Mo XXX, XXXI, and XXXII from a laser-produced plasma," J. Opt. Soc. Am. **67**, 1521 (1977).
13. G. E. Bromage, R. D. Cowan, and B. C. Fawcett, "Atomic structure calculations involving optimization of radial integrals: energy levels and oscillator strengths for Fe XII and Fe XIII $3p$–$3d$ and $3s$–$3p$ transitions," Mon. Not. R. Astron. Soc. **183**, 19 (1978).
14. E. Ya. Kononov, A. N. Ryabtsev, and S. S. Churilov, "Spectra of sodium-like ions Cu XIX–Br XXV," Phys. Scr. **19**, 328 (1979).
15. B. C. Fawcett and A. T. Hatter, "Spectra of the $3s^23p^n$–$3s3p^{n+1}$ transition arrays emitted from nickel and cobalt ions," Astron. Astrophys. **84**, 78 (1980).
16. M. Finkenthal, E. Hinnov, S. Cohen, and S. Suckewer, "The $3s^2\,{}^1S_0$–$3s3p\,{}^3P_1$ magnesium sequence intercombination lines from Sc X to Mo XXXI observed in the PLT tokamak," Phys. Lett. **91**, 284 (1982).
17. B. C. Stratton, W. L. Hodge, H. W. Moos, J. L. Schwob, S. Suckewer, M. Finkenthal, and S. Cohen, "Spectra of germanium and selenium in the 50–350 Å region from the PLT tokamak plasma," J. Opt. Soc. Am. **73**, 877 (1983).

18. J. Reader, "$3s^2$–$3s3p$ and $3s3p$–$3s3d$ transitions in magnesium-like ions from Sr^{26+} to Rh^{33+}," J. Opt. Soc. Am. **73,** 796 (1983).
19. N. J. Peacock, M. F. Stamp, and J. D. Silver, "Highly-ionized atoms in fusion research plasmas," Phys. Scr. **T8,** 10 (1984).
20. W. E. Behring, J. F. Seely, S. Goldsmith, L. Cohen, M. Richardson, and U. Feldman, "Transitions of the type $2s$–$2p$ in highly ionized Cu, Zn, Ga, and Ge," J. Opt. Soc. Am. B **2,** 886 (1985).
21. K. D. Lawson and N. J. Peacock, "The analysis of the $n = 2$–2 transitions in the XUV spectra of Cr to Ni," J. Phys. B **13,** 3313 (1980).
22. E. Hinnov, F. Boody, S. Cohen, U. Feldman, J. Hosea, K. Sato, J. L. Schwob, S. Suckewer, and A. Wouters, "Spectrum lines of highly ionized zinc, germanium, selenium, zirconium, molybdenum, and silver injected into Princeton Large Torus and Tokamak Fusion Test Reactor tokamak discharges," J. Opt. Soc. Am. B **3,** 1288 (1986).
23. J. Sugar and V. Kaufman, "Wavelengths and energy levels of Zn XII to Zn XX," Phys. Scr. **34,** 797 (1986).
24. M. Finkenthal, B. C. Stratton, H. W. Moos, W. L. Hodge, S. Suckewer, S. Cohen, P. Mandelbaum, and M. Klapisch, "Spectra of highly ionized zirconium and molybdenum in the 60–150 Å range from PLT tokamak plasmas," J. Phys. B **18,** 4393 (1985).
25. J. Reader, V. Kaufman, J. Sugar, J. O. Ekberg, U. Feldman, C. M. Brown, J. F. Seely, and W. L. Rowan, "$3s$–$3p$, $3p$–$3d$, and $3d$–$4f$ transitions of sodiumlike ions," J. Opt. Soc. Am. B **4,** 1821 (1987).
26. U. Feldman, L. Katz, W. Behring, and L. Cohen, "Spectra of Fe, Co, Ni, and Cu isoelectronic with Na I and Mg I," J. Opt. Soc. Am. **61,** 91 (1971).
27. B. Edlén, "Comparison of theoretical and experimental level values of the $n = 2$ complex in ions isoelectronic with Li, Be, O. and F," Phys. Scr. **28,** 51 (1983).
28. B. Edlén, "Comparison of theoretical and experimental level values of the $n = 2$ configurations in the boron isoelectronic sequence," Phys. Scr. **28,** 483 (1983).
29. B. Edlén, "Comparison of theoretical and experimental level values of the $n = 2$ configurations in the nitrogen isoelectronic sequence," Phys. Scr. **30,** 135 (1984).
30. B. Edlén, "Comparison of theoretical and experimental level values of the $n = 2$ configurations in the carbon isoelectronic sequence," Phys. Scr. **31,** 345 (1985).
31. B. Edlén, "Na-like spectra of the elements calcium through copper, K IX–Cu XIX," Z. Phys. **100,** 621 (1936).
32. I. P. Grant, B. J. McKenzie, and P. H. Norrington, "An atomic multiconfiguration Dirac-Fock package," Comput. Phys. Commun. **21,** 207 (1980).
33. J. F. Seely, J. O. Ekberg, U. Feldman, J. L. Schwob, S. Suckewer, and A. Wouters, "Wavelengths for the $3s^2\ {}^1S_0$–$3s3p\ {}^3P_1$ transition of the magnesiumlike ions Fe^{14+}–Nd^{48+}," J. Opt. Soc. Am. B **5,** 602 (1988).